Influence of Hydrogen Bonding on the Properties of Water Molecules Adsorbed in Zeolite Frameworks

A. V. LARIN,[1,2] D. N. TRUBNIKOV,[1] D. P. VERCAUTEREN[2*]

[1]*Department of Chemistry, Moscow State University, Leninskie Gory, Moscow, B-234, 119899, Russia*

[2]*Laboratoire de Physico-Chimie Informatique, Facultés Universitaires Notre Dame de la Paix, Rue de Bruxelles 61, B-5000 Namur, Belgium*

Received 3 May 2002; accepted 16 September 2002

DOI 10.1002/qua.10496

ABSTRACT: Three hydrated aluminosilicate frameworks—LiABW, NaNAT, and BaEDI—are partly optimized with the periodic Hartree–Fock CRYSTAL95 code. In particular, we optimized the positions of the adsorbed water molecules including the positions of the framework cations (ABW, NAT) or part of the framework atomic positions (ABW). This allowed us to compare cation–water clusters in the gas and adsorbed states and discuss the influence of hydrogen bonding to the framework oxygen atoms or to the neighbor water molecules on the atomic properties (quadrupole coupling constant, anisotropy of electric field gradient) of the adsorbed water molecules. The LiBIK structure obtained from X-ray diffraction is also considered to illustrate the hydrogen bonds occurring between adsorbed water molecules. Int J Quantum Chem 92: 71–84, 2003

Key words: zeolites; water molecules; hydrogen bonds; periodic Hartree–Fock; quadrupole coupling constant; electric field

Introduction

Most minerals and natural zeolites occur in hydrated forms. But, how strongly is water coordinated to the cations and how are their properties like the multipole moments (MMs) as well as their mobility influenced by the framework as compared to within dehydrated zeolites? The important experimentally measured electric field [1, 2] should a priori distort the H_2O molecules and enables us to evaluate easily their coordination on the basis of their characteristics in the gas state. But, does this distortion in the framework come from the electric field effects only or is it the result of different coordinations of each proton to the framework oxygens? Powder neutron diffraction and infrared spectroscopy have shown the appearance of H_3O^+ ions [3]. But, could theoretical studies of the H_2O

Correspondence to: D. Vercauteren; e-mail: daniel@cs.queensu.ca

*Current address: Department of Computing and Information Science, Queen's University, Goodwin Hall, Kingston, Ontario K7L 3N6, Canada.

This article was presented at the 42nd Annual Sanibel Symposium, February 23–March 1, 2002

localization in H-form zeolites confirm the appearance of H_3O^+ and is proton transfer possible to one H_2O molecule, or to H_2O dimers or clusters as obtained with the *ab initio* molecular dynamics (AIMD) approach by Jeanvoine et al. [4] or Termath et al. [5]?

If hydrogen bonding to the framework, $O_{zeol} \ldots H_{water}$, is the main reason of the water O—H bond length variation upon H_2O adsorption, then a shorter O—H bond should correspond to longer hydrogen bonds (HBs). However, the experimental structures of NaNAT [6] and LiABW [7] obtained via X-ray diffraction (XRD) do not show such behavior. Also, in the case of BaEDI solved by XRD [8] this criterion is fulfilled only for the two shortest O—H bonds out of four, even though all O—H bonds are short. For LiBIK, the protons with the shortest O—H bond are included into longer O . . . H HBs; all O—H distances are close while the O . . . H lengths vary within a wide interval between 1.9 and 2.6 Å [9].

One possible explanation for these discrepancies is that XRD measurements of hydrated zeolite crystalline forms cannot accurately fit the proton position. A unified application of the XRD and neutron diffraction data, for example under the form of constraints imposed on the H positions on the basis of neutron diffraction [10], is not always successful to combine the positional and displacement parameters coming from both techniques. The problem owes to the different thermal diffuse scattering and extinction effects in each of the techniques [10]. The help from quantum mechanical methods could thus be crucial to localize correctly the H_2O protons. Looking in this direction, the importance of long-range effects imposes the consideration of methods simulating periodic 3-D structures. Application of embedded and/or isolated clusters would indeed always hold the open question about the precision and/or importance of the long-range effects.

Elucidating the questions above mentioned on the importance of the HBs evidently requires the study of the interactions between H_2O, the zeolite cations, and the zeolite framework atoms for a wide set of structures. In this article, we compare experimental and theoretical 3-D hydrated zeolite models and the respective theoretical structures of cation/water clusters to understand the influence of the zeolite interactions on the structure of the adsorbed H_2O molecules.

The best choice of the most appropriate molecular or atomic properties to describe the changes upon adsorption is not easy. Surely, MMs can be interesting properties. MMs of H_2O linked to small peptides or adsorbed in NaNAT zeolite have, for example, already been carefully analyzed [11]. Such study revealed the variation of the H_2O dipole as compared to the gas state with a nonzero dipole component in the direction perpendicular to the H—O—H plane. This component is the largest for H_2O adsorbed in zeolite. Also, the variations of higher-order MMs, i.e., up to octupole, were shown to be large even if appreciable differences between the gas-state experimental and theoretical values hindered the evaluation more quantitatively the extent of these calculated changes in adsorbed and/or intercalated H_2O molecules. The dipole moment of H_2O chains was also the object of AIMD studies of H_2O adsorbed in 1-D channels in LiBIK and LiABW zeolites [12–14].

Quadrupole coupling constants C_{qq} of the ^{17}O and ^{2}H nuclei are other parameters that characterize the H_2O behavior in adsorbed and crystalline states. C_{qq} values for ^{17}O and ^{2}H were, for example, already calculated by the periodic Hartree–Fock (PHF) method [15] in various ice phases [16] and for ^{2}H in oxalic acid dihydrate [17]. More particularly, it was shown that the $C_{qq}(^{17}O, ^{2}H)$ were overestimated at the Hartree–Fock (HF) level and underestimated with density functional theory (DFT, equally with local and nonlocal functionals) for two ice VIII and IX crystalline phases [16]. This result was explained as due to shorter and longer O . . . O distances optimized at the HF and DFT levels, respectively. The authors also classified the factors influencing the $C_{qq}(^{17}O, ^{2}H)$ values of the H_2O molecules as owing to (1) the electric field from the neighbor molecules, (2) the polarization of the H_2O molecules due to this field, and (3) the O—H elongation accompanying (1) and (2). The authors mentioned that factor (3) is, however, negligible for $C_{qq}(^{17}O)$, but not for $C_{qq}(^{2}H)$ [16]. The latter was also confirmed for the O—H moieties in H-form aluminosilicates, for which a good agreement with known experimental $C_{qq}(^{2}H)$ values for relevant systems was proved at the PHF/ps-21G*(Al, Si)/6-21G*(O, H) level [18] owing to the inharmonic elongation of the O—H bridged group. Unfortunately, to our knowledge any correlation between the $C_{qq}(^{17}O)$ or the electric field gradient (EFG) anisotropy and the H—O—H bond angle of H_2O was never discussed.

In this article, we analyze the geometry distortions of adsorbed H_2O molecules due to hydrogen bonding in various cationic aluminosilicates and one H-borosilicate ABW form. In the first two parts,

TABLE I

O—H bond lengths in H_2O adsorbed in various zeolites and $O_z \ldots H_w$ or $O_w \ldots H_w$ HBs (Å), *w* and *z* being for H_2O and zeolite, respectively: X-ray diffraction (XRD), AIMD [14], and PHF-optimized zeolite models.

Zeolite	Model	O—H	O . . . H
LiABW	XRD [7]	0.955	2.004*w*
		1.096	2.169
	PHF	0.993	2.246*w*
		1.012	2.062
	AIMD [14]	0.989	2.162, 2.319*w*
NaNAT	XRD [6]	0.968	1.887
		0.974	2.060
	PHF	1.003	1.876
		0.995	2.062
BaEDI	XRD [8]	0.928	2.094
		0.942	2.103
		0.956	2.022
		0.959	1.915
	PHF	0.993	2.059
		0.993	2.096
		0.994	2.018
		0.995	1.882
LiBIK	XRD [9]	0.942	2.634
		0.949	2.002*w*
		0.953	2.609
		0.955	1.998*w*
	AIMD [14]	0.993	1.866*w*, 2.265
HABW(B)	PHF [22]	0.936	1.840, 1.927
		0.938	2.040

w, the $O_w \ldots H_w$ hydrogen bonds between the neighbor H_2O molecules.

we present the zeolite structures and computational details. The two following parts are devoted to the discussion of the C_{qq}, EFG anisotropy, and electric field values calculated with the CRYSTAL code [15] at the pseudopotential (ps) of Durant–Barthelat (Si, Al) or full electron (other elements) split-valence basis set. In the last part, the electron density critical points of (3, −3) and (3, −1) types obtained via AIM analysis [19] with the TOPOND96 code [20] are compared with those observed via cluster calculations with Gaussian 98 [21].

Zeolite Models

We will consider two types of zeolite structures, i.e., with HBs between the adsorbed H_2O molecules in the case of LiBIK and LiABW and without such HBs in the case of NaNAT and BaEDI (Table I). With the exception of long HBs of ~2.6 Å in LiBIK, the H_2O molecules present HBs with the frameworks. One "theoretical" H-form ABW borosilicate [22], including HBs between the adsorbed H_2O molecules as for LiABW, will also be considered. Various clustering of adsorbed particles have been observed in zeolite frameworks. Two examples from the literature, i.e., linear H_2O chains in LiBIK (Fig. 1) and an eight-membered ring H_2O geometry in BaEDI (Fig. 2), are presented below. In Figure 2(b), where we omitted the framework atoms, one

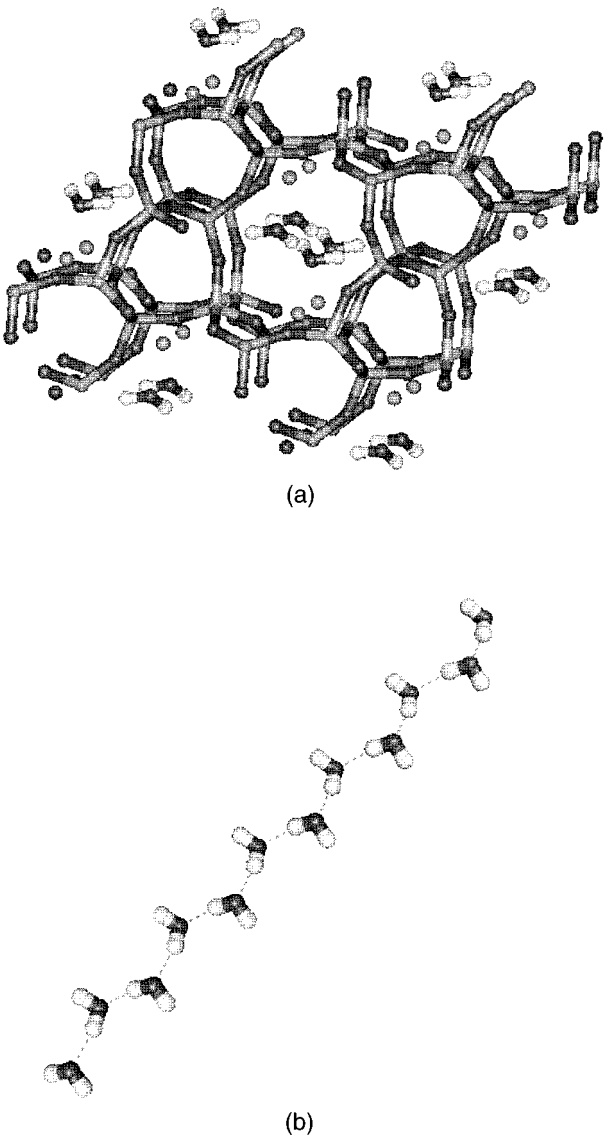

FIGURE 1. View of (a) LiBIK structure and (b) 1-D water chain extracted from the 8T channels [9]. Water—water hydrogen bonds are shown by broken lines.

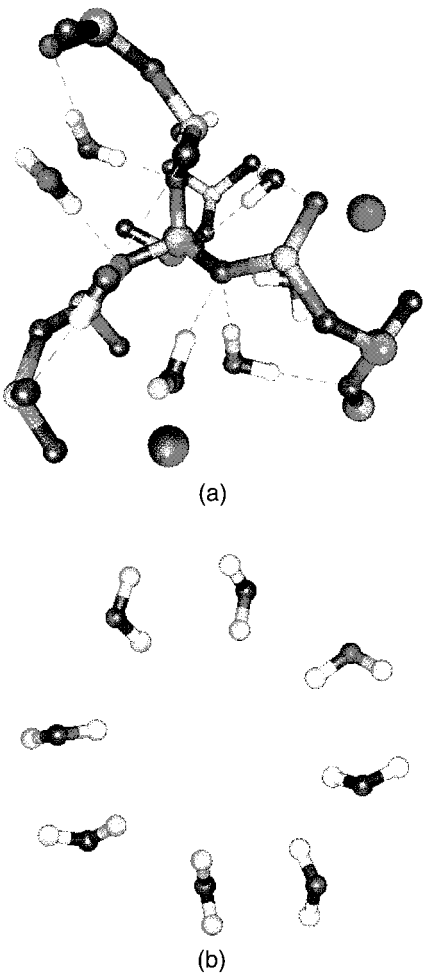

FIGURE 2. View of (a) BaEDI structure and (b) eight-ring water "cluster" extracted from the XRD model [8]. Zeolite—water hydrogen bonds are shown by broken lines.

can observe an eight-ring cluster with alternation of the O . . . O distances (2.997, 3.062, 2.924, and 3.062 Å) and O . . . O . . . O angles (129.4, 127.1, 128.6, and 127.1°). The principal difference between the cyclic H_2O cluster and the linear chains observed in LiBIK [Fig. 1(b)] is the presence of HBs with alternation (2.002, 1.997 Å) in the —(. . . H—O . . . H—O)— chain, the O . . . O distance (2.930 Å) being close to the smallest ones in the eight-ring cluster. One should add that the O . . . H distances in both types of structures are close to the values obtained by optimization of small H_2O clusters at the MP2(full)/6-311++G** level [23]. These O . . . H distances decrease from 1.951 Å in the H_2O dimer to 1.75 Å in the pentamer [23]. The chain HBs were the reason of the discussion by Quartieri et al. [24] on the existence of 1-D ice-like structures in the channels of the LiBIK zeolite. Indirectly, the proposition about the "ice-like" nature means that the O . . . H bonds between the H_2O molecules adsorbed in this structure even in 1-D are more important for the changes of the H_2O properties than the HBs to the framework oxygen atoms. This idea deserves a detailed theoretical study, which we performed in this work in comparison with another example of H_2O chain present in LiABW (Fig. 3). In the last case, one observes an "attached" chain whose half of the hydrogens are also linked to the framework oxygens.

Computational Strategy

Three "small" cationic aluminosilicate forms, i.e., LiABW, NaNAT, and BaEDI (Table II), were opti-

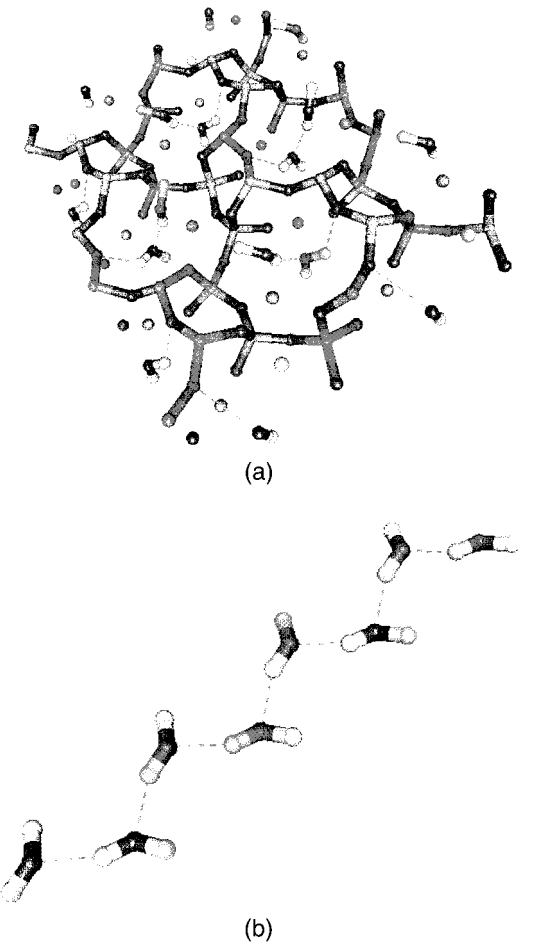

FIGURE 3. View of (a) LiABW structure [7] and (b) 1-D water chain extracted from the PHF model. Water—water and zeolite—water hydrogen bonds are shown by broken lines.

TABLE II

Symbol, number of atoms, of different Al, Si, and O types, of atomic orbitals (AO) per unit cell (UC), and symmetry group of the cationic forms of aluminosilicates and H-form ABW borosilicate.

Name	Symbol	Atoms/UC[a]	$n_{Al}/n_{Si}/n_O$	AO/UC[b]	Symmetry
LiABW	LiABW	28/40	1/1/4	464	$Pna2_1$
Natrolite	NaNAT	34/46	1/2/5	578	$Fdd2$
Edingtonite	BaEDI	32/56	1/2/5	628	$P2_12_12$
Bikitaite	LiBIK	20/26	2/4/12	304	$P1$
HABW	HABW	28/40	1/1/4	448	$Pna2_1$

[a] For dehydrated/hydrated forms.
[b] Hydrated form at the PS-21G** level.

mized at the STO-3G level for the framework atoms and 6-1G, 8-511G, and pseudopotential Hay–Wadt (small core or HWSC) basis sets for the Li, Na, and Ba cations (with *d* polarization functions), respectively, with the periodic PHF CRYSTAL95 code [15], in which we adopted the Polak–Ribiere algorithm [25]. PHF optimizations were performed for the cations and H_2O atoms for NaNAT and for the H_2O atoms only for BaEDI. For LiABW, the three cell parameters and coordinates of Li, O_2, O_3, and O_4 atoms were optimized. Series of small $Me^{+n}(H_2O)_m$ clusters, Me = Li, Na, and Ba, were also considered with Gaussian 98 [21] to estimate the basis set quality used with the PHF approach.

To calculate the properties and verify the relative energies of the initial and optimized structures at a higher basis set level, single-point calculations for all three structures, plus LiBIK, were performed at the pseudopotential (ps-21) Durant–Barthelat basis level for Si and Al, denoted below as the ps-21G** and ps-21G* with and without *d* polarization functions for the cations mentioned above, and at the 6-21G* level for H and O. The used *sp*/*d* exponents were 0.9, 0.12339/0.5, 0.17/0.45, and 0.3737/0.6 a.u.$^{-2}$ on the H, Al, Si, and O atoms, respectively. The *d* exponents on Li, Na, and Ba were 0.8, 0.175, and 0.33 a.u.$^{-2}$, respectively.

To search all the critical points (CPs) of the electron density with the TOPOND96 code for LiABW and HABW(B), we varied the number of cluster atoms (until 12) around each crystallographically independent type of atom, the number of maximum steps of the search (up to 80), and the maximum radius of the cluster (until 10 Å). The largest set of CPs was obtained with 8 atoms, 50 steps, and 8 Å, respectively. Even if 40 steps looked sufficient, the shift from 40 to 50 allowed us to find one additional CP for the PHF model of LiABW.

All computations with the CRYSTAL95 and Gaussian 98 codes were carried out on an IBM 15-node (120-MHz) scalable POWERparallel platform (1 Gb of memory/CPU) with conventional tolerance criterions. The total PHF geometry optimization of the hydrated LiABW form (27 variables) with the 6-1G(Li)/STO-3G(Al, Si, O, H) basis set took nearly 670 h on the above-cited CPU. A single-point calculation for the LiBIK structure, which is relatively small but has no symmetry (P1 group), requires 34 min at the 6-1G(Li)/STO-3G(Al, Si, O, H) level; we did not optimize it with CRYSTAL. For visualization, we used the MOLDRAW 2.0A code [26].

Results

OPTIMIZED MODELS

The PHF geometry optimization with 6-1G/STO-3G of a relatively crude initial XRD model for LiABW including H_2O molecules resulted in an energy gain of 75.9 kcal/mol, which is supported by a coherent value of 54.8 kcal/mol with 6-1G*/ps-21G*. One should also mention a previous application of CRYSTAL in which we tackled the "dehydration" of LiABW, leading to a reasonable decrease of the cell volume by 1.5% [27] opposite the increase by 5% calculated with a force field available in Cerius 2.4 [28].

For NaNAT, the optimization with STO-3G led to an energy decrease of 13.8 kcal/mol, but single-point calculations at the 8-511G*/ps-21G* level showed that the XRD [6] model is more stable by 3.1 kcal/mol than the PHF model optimized with the minimal basis set. Attempts to achieve more stable models varying only the H coordinates

TABLE III

Coordination of the cation to the zeolite framework atoms and geometry of the $Me^{+n}(H_2O)_m$ clusters (n = 1 for Li and Na, 2 for Ba; m = 1, 2, and 4 for Li, Na, and Ba, respectively): experimental data (XRD), periodic models optimized with CRYSTAL (PHF), AIMD with Becke exchange and Perdew correlation functionals [14], and cluster models optimized with Gaussian 98 (G98).

Me	Method	$R_{Me—O}$ (Å)[a]	R_{OH} (Å)	H—O—H (°)
Li	LiABW, XRD [7]	1.913, 1.968*w*, 1.981, 1.942	0.955, 1.096	126.4
	PHF/6-1G/STO-3G[b]	1.814*w*, 1.878, 2 × 1.942	1.012, 0.993	105.4
	AIMD [14]	—	2 × 0.989	106.8
	G98/6-1G*/6-21G*	1.724	0.955	103.8
	G98/MP2/6-1G*/6-21G*	1.722	0.972	102.1
	G98/MP2/6-311+G**	1.866	0.965	105.0
Na	NaNAT, XRD [6]	2.367, 2.370*w*, 2.391*w*, 2.395, 2.518	0.974, 0.968	114.0
	PHF/8-511G/STO-3G[c]	2.345*w*, 2.368, 2.380, 2.382*w*, 2.512	1.003, 0.995	109.2
	G98/8-511G/STO-3G[d]	2.022	0.981	103.7
	G98/8-511G*/6-21G*[d]	2.096	0.955	103.2
	G98/8-511G*/6-21G*[d]	2.370, 2.391 (fixed)	0.954	103.3
	G98/MP2/8-511G*/6-21G*[d]	2.104	0.974	101.4
	G98/MP2/6-311+G**[e]	2.290	0.963	103.9
Ba	BaEDI, XRD [8]	2 × 2.792*w*, 2 × 2.788*w*	0.959, 0.928, 0.942, 0.956	2 × 101.7, 2 × 111.3
	PHF/HWSC3-1G*/STO-3G[f]	2 × 2.729*w*, 2 × 2.746*w*	0.993, 0.994, 0.993, 0.995	2 × 100.9, 2 × 104.1
	G98/LANL2MB*/6-21G*[g]	4 × 2.631	4 × 0.958	4 × 105.2
	G98/B3LYP/LANL2MB*/6-311+G**[h]	4 × 2.720	4 × 0.969	4 × 104.1
	Experiment (gas phase)		0.959	103.9

Basis set first notation is for the Me ion followed by the one on the other atoms.

[a] *w* denotes distance to H_2O oxygens (*w* is omitted in the cluster calculations).

[b] PHF optimization of all cell sizes and all atomic coordinates.

[c] PHF optimizations of Na^+ and H_2O coordinates only.

[d] Cluster optimization with fixed $O_w \ldots Na^+ \ldots O_w$ angle of 141.2°.

[e] Cluster optimization allowing variation of $O_w \ldots Na^+ \ldots O_w$ angle up to 180°.

[f] PHF optimization of H_2O coordinates.

[g] Partial cluster optimization upon fixed O_w—Ba^{+2}—O_w angles corresponding to the XRD case.

[h] Total cluster optimization with pseudopotential LANL2MB basis set including 31 split-valence [21] plus *d* functions on Ba^{+2}, resulting in $O_w \ldots Ba^{+2} \ldots O_w$ angles 2 × 110.6, 2 × 110.7, 107.1, 107.2° close to tetrahedral values.

(without Na cation) were not successful, the resulting structure having a higher energy as compared to the initial XRD model by 2.0 kcal/mol. Even if the initial and optimized NaNAT geometries were close (Table III), significant differences were observed between the atomic charges calculated here and via multipole X-ray fitting [6]. The O charges calculated with the higher-quality basis set are closer than those at the STO-3G level. The experimental estimate of the charge of the H_2O molecule, +0.01 e [6], is contrary to the negative value of −0.07 and −0.01 e calculated at the 8-511G/ps-21G* and 8-511G*/ps-21G* levels, respectively. The H charges are also closer to each other than the experimental ones. More information about the charge distribution is given in Ref. [27].

After optimization, the shorter O—H lengths in H_2O correspond to a longer respective $O_w \ldots H$ hydrogen bond (w corresponding to H_2O) in the case of H_2O adsorbed in LiABW and NaNAT; the situation is similar for the optimized H_2O molecules adsorbed in BaEDI. The increase of the $O_w \ldots H$ hydrogen bond length by 0.24 Å in the LiABW structure is not a consequence of the known overestimated HBs obtained by HF calculation [16] as the coordinates of the Li and O framework atoms

plus the cell parameters were varied and the HBs can hardly play an essential role in the total energy variation. Let us add that the increase of the $O_w \ldots H$ distance with the AIMD optimization varying all fractional coordinates upon fixed-cell LiABW parameters was even larger, i.e., up to 2.319 Å (Table I) [14]. Their optimization holds the $O_z \ldots H$ distance as 2.162 Å (z corresponding to zeolite) opposite the decrease from 2.169 in the XRD model to 2.062 Å in the PHF one.

So far, PHF optimizations of most zeolite models can only be done with a low-quality basis set, which, unfortunately, can lead to a distorted optimized structure. To verify the influence of the basis set level on the relative location of the H_2O molecules vs. the zeolite cation, we compared the PHF-optimized structures with isolated charged $Li^{+1}(H_2O)$, $Na^{+1}(H_2O)_2$, and $Ba^{+2}(H_2O)_4$ clusters extracted from the crystalline XRD structure, hence without any environment (Table III). The Li cluster will also be used later for the characterization of the CPs.

The dependence of the basis set used on the H_2O geometry and of the geometry restrictions, i.e., fixed Me—O distances and/or O—Me—O angles, upon optimization will only be illustrated in detail for the $Na^{+1}(H_2O)_2$ case. The same tendencies were revealed for the Li and Ba water clusters. There are four Na atoms and four H_2O molecules in NaNAT per unit cell (UC), one of the H_2O molecules being in contact with a Na of the neighbor UC. It is worth mentioning that the water O—H distance and the H—O—H angle optimized at the same level of basis set as shown for the Na cluster with 8-511G*/6-21G* basis set do not vary with the Me . . . O distance (optimized or fixed) (Table III). The O—H length in the cluster at the STO-3G level is shorter than in the optimized zeolite model by 0.01–0.02 Å despite the fact that the $Na^+ \ldots O$ distance is shorter by 0.32 Å for the same $O \ldots Na^+ \ldots O$ angle (Table III). The Me . . . O distance does not vary between the MP2 (2.104 Å) or HF (2.096 Å) levels with the same 8-511G*/6-21G* basis used in single-point PHF calculations. The more advanced 6-311+G** basis leads to closer Me . . . O distances in both the cluster (2.290 Å) and PHF-optimized (2.345 Å) models, i.e., close to the sum of van der Waals (vdW) radii (O = 1.35, Li^+ = 0.56, Na^+ = 0.98, Ba^{+2} = 1.35 Å), with the exception of the $Li^+ \ldots O$ one. It is known that isolated clusters could lead to exaggerated electrostatic effects in the absence of field "compensating" zeolite oxygen atoms. Hence, the insensitivity of the O—H lengths in $Na^{+1}(H_2O)_2$ with respect to the Na . . . O distance variation could serve as an upper evaluation for the H_2O behavior in the NaNAT zeolite. This insensitivity confirms the minor distortion due to the electrostatic field or O—H bond polarization. The changes of the water H—O—H angle upon optimization with respect to the initial value show the tendency to approach the nearly equilibrium gas-state value of 104°. A larger angle deflection from the gas-state value, i.e., 109°2, is observed for H_2O in NaNAT.

In all three Li, Na, and Ba cation H_2O clusters, the use of the STO-3G basis on all atoms (with the exception of the cation) led to a longer O—H bond length with respect to the values calculated for the clusters at the level of the basis used for the single-point PHF calculations, i.e., 6-21G*(O, H). The latter difference can explain why the optimized NaNAT and BaEDI models have less stable total energies than the initial XRD ones at the 6-21G* level.

For BaEDI, the optimized structure was more stable at the STO-3G level by 34.1 kcal/mol, while the initial geometry was favored at the ps-21G** level by 14.1 kcal/mol. The BaEDI XRD structure corresponds to a distorted pyramid with $O \ldots Ba^{+2} \ldots O$ angles of 66.3, 118.6, 72.7, and 65.2°, the largest angle being between the two H_2O molecules closest to Ba. The PHF optimization of the H_2O coordinates changes only slightly the geometry up to 64.6, 118.3, 72.0, and 66.4° angles, close to a local minimum with a "pyramid" $Ba^{+2}(H_2O)_4$ geometry. However, the global minimum was revealed for a tetrahedral cluster symmetry (Table III). Even if only $Ba^{+2}(H_2O)_6$ hexamers and higher homologs were observed experimentally [29], the tetrahedral symmetry cannot be excluded allowing the energy difference of 3.9 kcal/mol between the octahedral $Ba^{+2}(H_2O)_6$ and "tetrahedral" $Ba^{+2}(H_2O)_4(H_2O)_2$ configurations, the last one including two H_2O molecules in the second solvation shell [30].

To "compensate" for the H_2O distortions appearing when optimizing the H_2O/zeolite models with the STO-3G basis set, we proposed to scale the geometry of the adsorbed H_2O molecules. Owing to the known longer O—H bond lengths calculated with STO-3G, the scaling procedure requires a shortening to provide a minimum of the total energy. To determine the scaling parameter for the O—H distance, we optimized the isolated H_2O molecule with the STO-3G and the 6-21G*(H, O) basis sets using Gaussian 98, which led to O—H values of 0.989 and 0.949 Å, respectively. It thus

TABLE IV

Energy variation (kcal/mol) of the BaEDI PHF-optimized structure relative to the energy of the initial XRD model [8] with respect to the scaling factor $s = |O—H|_{STO-3G}/|O—H|$ 6-21G* for the O—H bond length of adsorbed H_2O calculated with the HWSC*(Ba)/*ps*-21G*(Si, Al)/6-21G*(O, H) basis set at fixed positions of the H_2O oxygen atoms.

Energy variation	14.1	2.9	−1.2	−1.6	−1.1
Scaling factor	1.0	1.02	1.0352	1.0422	1.05

The value $s = |O—H|_{STO-3G}/|O—H|_{6-21G^*} = 1.0422$ at the energy minimum is the ratio of the O—H bond lengths obtained with both the basis sets (given by index) considered for the optimization of the isolated H_2O molecule.

resulted in a scaling parameter $s = |O—H|_{STO-3G}/|O—H|_{6-21G^*}$ of 1.0422. For the BaEDI model, the shortening of the O—H lengths by 1.0422 (the H—O—H angle being kept fixed) at fixed PHF-optimized O_w positions for all H_2O molecules led to a more stable system by 1.6 kcal/mol as compared to the initial XRD model (Table IV). The scaled O—H bond lengths of H_2O adsorbed in BaEDI hence range between 0.959 and 0.961 Å vs. the too long 0.993–0.995 Å range obtained previously (Table III).

In future work, we will only consider H_2O properties that are deduced from optimized and "O—H rescaled" NaNAT and LiABW models, as performed for the BaEDI case explained above. In this article, we will, however, concentrate on the comparison between the water properties calculated for both the XRD- and PHF-optimized models.

CALCULATED C_{qq} AND ELECTRIC FIELD GRADIENT ANISOTROPY

To assess the difference between the experimental H_2O properties and the ones calculated with the 6-21G*(O, H) basis set, we first computed the C_{qq} values of the ^2H and ^{17}O atoms of H_2O in the gas-state geometry. The calculated values ("+" signs in Fig. 4 for ^2H and star sign in Fig. 5 for ^{17}O; it coincides with the upper values for BaEDI) are higher than the experimental ones (upper open square and open square in Figs. 4 and 5, respectively). The difference, i.e., around 10% for ^2H and 16% for ^{17}O, is largely smaller than the one obtained for the ^2H atoms with PHF/6-21G* for the α- or β-phases of oxalic acid dihydrate, i.e., 40 and 52% in α- and β-phases, respectively [17]. For comparison, we also calculated the gas-state $C_{qq}(^2H)$ values for O—H distances ranging from 0.94 to 1.09 Å ("+" signs in Fig. 4) at a fixed HOH angle of 104°. (Note: it has been shown that the variation of the H_2O valence angle does not influence the $C_{qq}(^2H)$ values [17].)

Our PHF treatment of the 1-D water chain in LiBIK has been undertaken on the structure extracted out of the zeolite 8T channel, i.e., without any zeolite atoms. We used the structure from Ref. [9] because the reported H_2O geometry is less distorted than the one in Ref. [24], where too short OH bonds of 0.85 and 0.90 Å were obtained. In Figure 4, one can observe a sharp partitioning of four ^2H atoms into the "nonchain" ones (C_{qq} = 0.416 and 0.389 MHz) and "chain" ones (C_{qq} = 0.360 and 0.346 MHz). The two upper values are close to the values calculated for H_2O in the gas state (C_{qq} = 0.389 MHz at |O—H| = 0.954 Å given by "+" sign in Fig. 4 for H_2O calculated with 6-21G*).

The $C_{qq}(^2H)$ differences between the two types of ^2H atoms of the 1-D chain model extracted from the LiBIK decreases while considering the whole sys-

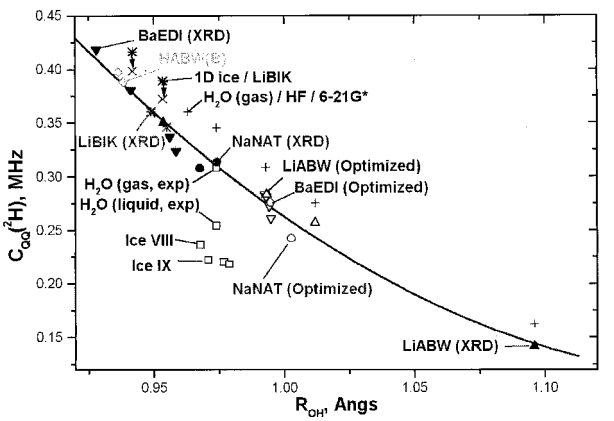

FIGURE 4. Quadrupole coupling constants C_{qq} at the ^2H atoms of H_2O adsorbed in zeolites (solid signs and "X", cationic form aluminosilicate models resolved by XRD; open signs, PHF-calculated models), H_2O in the gas state (highest open square, experimental value at |OH| = 0.974 Å; plus sign, calculated at various |OH| values), ice VIII and IX (squares, experimental [16]), and 1-D water chain extracted from the LiBIK zeolite (stars, PHF-calculated model) with respect to OH distance. The quadratic curve is fitted over all LiABW, BaEDI, and NaNAT data.

tem, i.e., water and zeolite framework. $C_{qq}(^2H)$ values are changed for the "nonchain" ^2H atoms only (from C_{qq} = 0.416 and 0.389, given by "*" signs, to 0.398 and 0.372 MHz, given by "X" signs, following the arrows in Fig. 4), the "chain" ^2H holding their positions (from C_{qq} = 0.360 and 0.346 to 0.359 and 0.345 MHz) on the curve fitted for all water ^2H atoms in the three structures—LiABW, NaNAT, and BaEDI. Approximately, the influence of the HBs toward the framework leads to "chain" ^2H type as in neighbor H_2O molecules linked by hydrogen bonding. It suggests that adsorbed H_2O is closer to the "ice" state in the presence of hydrogen bonding.

Another reasonable consequence of the geometry optimization can be observed by analyzing the behavior of the EFG anisotropy η at the ^{17}O nuclei. Although it could be useful, this parameter was, to our knowledge, never discussed. We observe a correlation of $\eta(^{17}O)$ with the water H—O—H valence angle, not considering the large H—O—H angle (126°4) in the XRD model of LiABW (Fig. 6). This dependence also supports the idea of the local nature of the EFG at the H_2O nuclei. The $C_{qq}(^{17}O)$ values calculated in the PHF-optimized models, i.e., with smaller H—O—H angles than in the XRD initial models, are reasonably larger (see arrow in Fig. 5) but do not show the same evident correlation with the H—O—H angle as for the $\eta(^{17}O)$ values

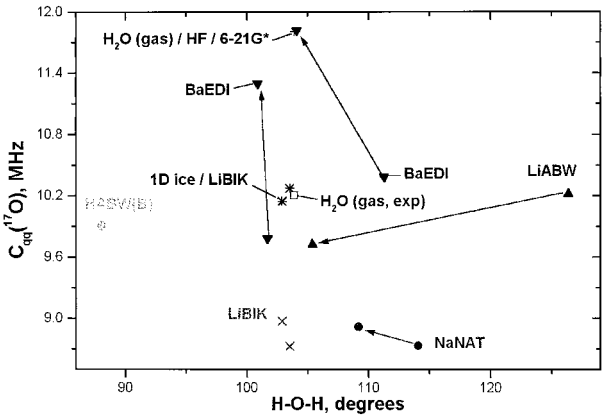

FIGURE 5. Quadrupole coupling constants C_{qq} at the ^{17}O atoms of H_2O adsorbed in zeolites (filled signs and "X", cationic form aluminosilicates; diamond, H-form ABW borosilicate), H_2O in the gas state (open square, experimental value at |OH| = 0.974 Å; plus sign, calculated at HOH = 103.9° and |OH| = 0.936 Å), and 1-D water chain extracted from the LiBIK zeolite (stars, PHF-calculated model) with respect to HOH angle. The changes upon optimization are shown by arrows.

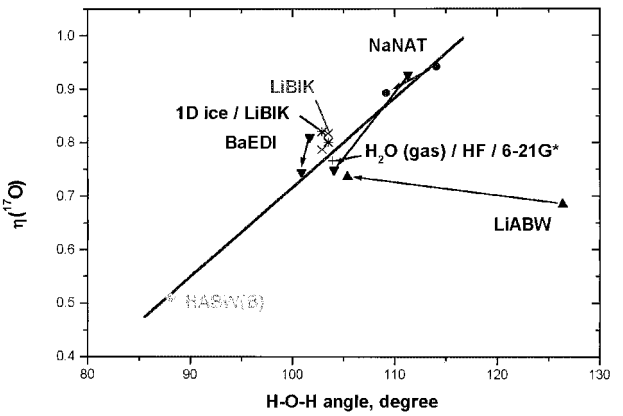

FIGURE 6. Electric field gradient anisotropy η at the ^{17}O atoms of H_2O adsorbed in zeolites (solid signs and "X", cationic form aluminosilicates; diamond, H-form ABW borosilicate), H_2O in the gas state (plus sign, calculated at 0.968 Å and 104°), and 1-D water chain extracted from the LiBIK zeolite (stars, PHF-calculated model) with respect to HOH angle. The changes upon optimization are shown by arrows.

(Fig. 6). Again, the variation of the $C_{qq}(^{17}O)$ values in LiABW upon optimization has an opposite behavior as compared to those of BaEDI and NaNAT. The peculiar difference for the $C_{qq}(^{17}O)$ and $\eta(^{17}O)$ values in LiABW could be assigned to a strong change in the electron molecular density at large H—O—H angle (126°4).

ELECTRIC FIELD AT THE H AND O ATOMIC POSITIONS

The electric field (EF) at the proton after optimization (Fig. 7) presents a particular behavior. Irrespective of the initial EF values obtained for the experimentally determined XRD models, the final values for the different optimized zeolite models are concentrated (see arrows in Fig. 7) in a narrow interval between 0.02 and 0.03 $E_h/(e \times a.u.)$. The only exception is for the proton with the longest O—H bond, i.e., in the XRD model of LiABW, whose EF changed from 0.1 to 0.045 $E_h/(e \times a.u.)$. This deviation of the EF in LiABW could also be explained by a more pronounced EF near the Li cation as compared to near the larger Na and Ba ones, whose EFs are in general lower. A larger EF of 9.5 V/mn = 1.85×10^{-2} $E_h/(e \times a.u.)$ within LiZSM-5 [31] was recently obtained using the CO probe molecule as compared to 1.22×10^{-2} in NaZSM-5 and 0.64×10^{-2} $E_h/(e \times a.u.)$ in RbZSM-5 [32], which are close to the ones measured in the

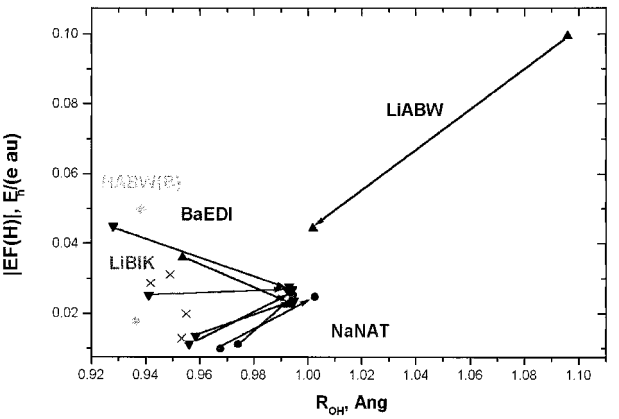

FIGURE 7. Electric field at H atoms of H_2O adsorbed in zeolites (filled signs and "X", cationic form aluminosilicates; diamond, H-form ABW borosilicate) with respect to OH distance. The changes upon optimization are shown by arrows.

respective forms of zeolite Y, i.e., 0.99×10^{-2} and 0.47×10^{-2} $E_h/(e \times a.u.)$ for NaY and NaRbY [2].

The EF values produced at the ^{17}O positions by the neighbor H_2O molecules in the 1-D chains extracted from the LiBIK zeolite, i.e., without considering any zeolite atoms, is high. In particular, the EF computed at the H_2O oxygens in the periodic H_2O chains is larger [0.1574 and 0.1568 $E_h/(e \times a.u.)$; stars in Fig. 8] than the EF computed at the same H_2O oxygen atoms considering also the zeolite framework [0.1402 and 0.1400 $E_h/(e \times a.u.)$; "X" signs in Fig. 8). The large difference between the two EF(H) in HABW [0.0498 and 0.0177 $E_h/(e \times a.u.)$; diamonds in Fig. 7] comes from the close position between one of the H_2O protons and two of the framework oxygens (1.840 and 1.927 Å in Table I).

Let us remark that, in another work [22] we also calculated the |EF(H)| values at the protons of bridged hydroxyl moieties for a series of PHF-optimized H-form aluminosilicates (ABW, CAN, CHA, EDI, and NAT) [18, 33, 34] as well as for ABW borosilicates [22]. Comparing the values, we observe that the |EF(H)| values for the various zeolite framework hydroxyl protons are different; the values range from 0.05 as for HNAT to 0.005 $E_h/(e \times a.u.)$ for HABW borosilicate, in opposite to the close EF values at the H_2O protons in the different zeolites. The narrow EF interval observed for H_2O is due to the strong local nature of the EF at the H_2O protons and as a result of the EF dependence on the water O—H bond length. All O—H distances are close for all PHF models optimized herein. It thus signifies that all the H_2O protons of the PHF models "feel" nearly the same EF. This suggestion is confirmed by the correlation between the water H—O—H valence angle and the EF values at the H_2O oxygen (approximate function given by the broken line in Fig. 8). This "|EF(O)| − HOH" correlation supports the local character of the EF(O).

The |EF(O)| is also a more important factor than the |EF(H)| for the resulting energy of the interaction between adsorbed H_2O and the zeolite framework due to the higher polarizability of the O vs. H atom. The inductive term proportional to the O polarizability and the |EF(O)| value contributes more to the total energy and is thus more important for the determination of the favored adsorbed H_2O position. Hence, we suggest that the |EF(O)| value is determined mainly by the closest H atoms in the same H_2O molecule and not by the closest zeolite atoms. It means that the |EF(O)| from the external zeolite atoms is not the dominating factor that drives the molecule to a favored position in the PHF-optimized models. This important suggestion could, however, deserve deeper analysis as it could be criticized from two sides: First, the choice of "small size" zeolites logically avoids the localization of H_2O molecules in large cavities where the situation could deviate from the one presented herein. Second, the PHF-optimized models of NaNAT and BAEDI (without rescaling; see text above) are less stable than the XRD initial models calculated at a higher basis set level. However, it

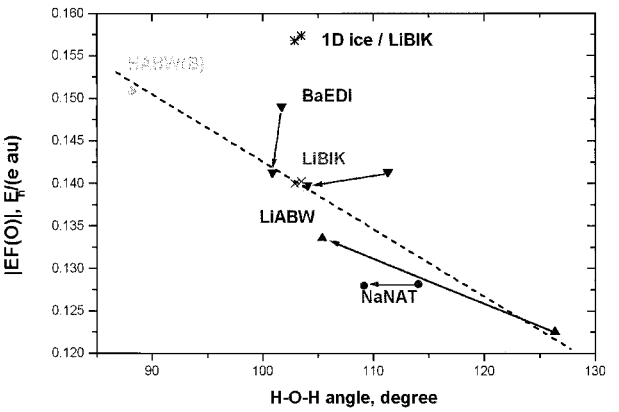

FIGURE 8. Electric field at the O atom of H_2O adsorbed in zeolites (filled signs and "X", cationic form aluminosilicates; diamond, H-form ABW borosilicate) and 1-D water chain extracted from the LiBIK zeolite (stars, PHF-calculated model) with respect to HOH angle. The changes upon optimization are shown by arrows. Linear approximation for all zeolites, with exception of the 1-D ice model, is given by the broken line.

seems that the first of the factors would be more important to tackle in further studies because the EF values for both XRD and PHF models of NaNAT are not that different.

The improvement of the basis set for the PHF optimization seems not to change qualitatively the local character of the EF on the nuclei. The application of a higher-quality basis set should lead to a shorter water O—H bond length that results in a higher EF value owing to a closer position of the neighbor atoms in the same molecule. This EF increase should dominate over the possible change of the EF at the H or O positions produced by the variation of the favored adsorbed molecular location (with a higher-quality basis set) with respect to the zeolite atoms. The simultaneous EF shift cannot be large because the distance between the H_2O and the nearest cation, which has a large contribution in the EF, is nearly equal to the sum of the vdW radius of the cation and oxygen in all the models applied herein.

TOPOLOGICAL CHARACTERIZATION OF HYDROGEN BONDS

The positions of all the bond CPs of the electron density, i.e., the (3, −1) CPs or passes, in LiABW and borosilicate HABW zeolites were calculated in accordance with Bader's criterion [19] as implemented in the TOPOND96 code [20]. This "small" ABW zeolite was ideal for such type of analysis as it includes HBs of the three types, i.e., water—water and water—zeolite (LiABW) (Fig. 3) as well as the bridged H—water (HABW). One obtained 46 and 44 bond CPs for the initial XRD and optimized PHF models of LiABW, respectively. None of the two (3, −3) CPs, or peaks, at the H atom in the HABW and only one of the two peaks in the XRD model of LiABW for the H with a longer O—H bond could be resolved. Irrespective of this, Morse's rule [19] for the summation of peaks, passes, pales, and pits was satisfied: $9 - 18 + 14 - 5 = 0$ and $10 - 18 + 12 - 4 = 0$ for the XRD and PHF models, respectively. For the optimized ABW framework, wherein the water O—H bond lengths are longer, both the proton peak CPs were resolved. Their electronic and geometric characteristics were similar and comparable to the one of the peaks in the initial XRD model. The hindrance to determine the O—H bond CPs comes from the short O—H bond as confirmed by the analysis of the $AlPO_4$-15 structure including H_2O molecules with O—H bond lengths ranging from 0.837–0.951 Å [35]. None of the peaks on the H_2O protons could be determined therein. For all peaks at the H_2O protons found in LiABW, the maxima of the electron density are displaced from the H positions by 0.13–0.14 Å, much larger than in the $Li^+(H_2O)$ cluster or isolated H_2O, i.e., nearly 0.028 and 0.026 Å, respectively, with the same configuration as in the LiABW zeolite.

The $Li^+(H_2O)$ cluster was analyzed with the AIM option in Gaussian 98 and two maximum bond CPs were determined. The total H_2O electronic density is not perturbed by contributions from the neighboring zeolite atoms and its topological analysis seems to be more simple for the isolated cluster situation. For the larger $Na^+(H_2O)_2$ and $Ba^{+2}(H_2O)_4$ clusters, we encountered the well-known problem of insufficient number of iterations with AIM.

Evidently, we paid more attention to the bond CPs between the H atoms of H_2O and the zeolite oxygens to characterize the H_2O proton coordination in their adsorbed state. Surprisingly, TOPOND96 allows us to determine bond CPs that are separated by distances of nearly 3 Å between the H and O atoms (Table V). Evidently, we can neglect these points comparing the relatively low electron densities at the CP position. The H . . . CP and O . . . CP distances are either close or slightly larger than those systematically observed for a large series of small peptides [11], i.e., from 0.28–0.71 Å for H . . . CP and from 1.02–1.35 Å for O . . . CP. From Table V, note that the parameters of the water—water and zeolite—water HBs are close in all aspects, with the exception of the bond ellipticity, before and after optimization of the LiABW zeolite. The close parameter values for both types of HBs (Table V) allow us to propose an equal influence of HB of any type, i.e., to the neighbor H_2O or to the zeolite oxygen, on the H_2O electronic properties. The minor differences between the HBs studied here could be assigned to the differences in the O_{zeol} . . . H and O_{water} . . . H bond lengths.

Conclusions

The observation of chains of H_2O molecules linked by HBs by Quartieri, Fois, and colleagues [12–14, 24] initiated the discussion of 1-D ice-like structures in zeolite channels. To verify this proposition, we considered a series of adsorbed H_2O molecules with O . . . H HBs between the H_2O molecules as in LiBIK and LiABW, as well as without

TABLE V

CPs of the electron density calculated with the TOPOND96 code [20] and Gaussian 98 [21] for the bonds between the H atoms of H_2O adsorbed in LiABW (XRD and PHF models), of isolated H_2O, of H_2O in the $Li^+(H_2O)$ cluster extracted from the LiABW zeolite model, and of H-form borosilicate HABW(B).

Type	$\|O_xH_y\|$	$\Sigma\|$X-CP$\|$	$\|H_y$-CP$\|$	$\|O_x$-CP$\|$	ρ(CP)	$\nabla^2\rho$(CP)	ELLI
LiABW/XRD/PHF/ps-21*(Si, Al)/6-21G*(O, H)/6-1G*(Li)/TOPOND96							
O_w—H_1	1.096	1.096	0.245	0.851	0.247	−1.191	0.026
O_z . . . H_1	***2.169***	***2.176***	***0.798***	***1.378***	***0.014***	***0.060***	***0.103***
O_z . . . H_1	2.807	3.048	1.303	1.745	0.002	0.009	1.088
O_w . . . H_1	2.993	3.412	1.627	1.785	0.001	0.008	2.416
O_w . . . H_2	***2.004***	***1.967***	***0.650***	***1.317***	***0.019***	***0.082***	***0.036***
O_z . . . H_2	2.998	3.077	1.317	1.760	0.002	0.013	1.447
H_2O/XRD/MP2(Full)/6-311G**/AIM							
O_w—H_1	1.096	1.096	0.426	0.670	—	−1.289	0.027
O_w—H_2	0.953	0.953	0.286	0.667	—	−2.671	0.024
$Li^+(H_2O)$/XRD/MP2(Full)/6-311G**/AIM							
O_w—H_1	1.096	1.096	0.380	0.716	—	−1.454	0.021
O_w—H_2	0.953	0.953	0.263	0.690	—	−2.722	0.019
LiABW/PHF/PHF/ps-21*(Si, Al)/6-21G*(O,H)/6-1G*(Li)/TOPOND96							
O_w—H_1	1.012	1.012	0.191	0.821	0.313	−2.445	0.027
O_z . . . H_1	***2.162***	***2.172***	***0.830***	***1.342***	***0.016***	***0.077***	***0.149***
O_z . . . H_1	2.783	3.076	1.315	1.761	0.001	0.008	2.068
O_z . . . H_1	3.071	3.118	1.330	1.788	0.001	0.009	0.363
O_w—H_2	0.993	0.994	0.168	0.826	0.330	−3.084	0.023
O_w . . . H_2	***2.246***	***2.247***	***0.828***	***1.420***	***0.011***	***0.055***	***0.023***
HABW(B)/PHF/PHF/ps-21*(Si)/6-21G*(O,B,H)							
O_w . . . H_{1b}	1.625	1.634	0.541	1.093	0.060	0.158	0.076
O_z . . . H_2	1.927	1.951	0.778	1.173	0.034	0.173	0.512
O_z . . . H_2	2.402	2.412	0.922	1.490	0.008	0.043	7.281
$Li^+(H_2O)$/PHF/HF/6-21G*(O,H)/6-1G*(Li)/AIM							
O_w—H_1	1.012	1.012	0.154	0.858	—	−2.206	0.031
O_w—H_2	0.993	0.993	0.074	0.919	—	−2.848	0.028
$Li^+(H_2O)$/PHF/MP2(Full)/6-311G**/AIM							
O_w—H_1	1.012	1.012	0.380	0.632	—	−2.181	0.021
O_w—H_2	0.993	0.993	0.263	0.730	—	−2.394	0.020

The |OH| bond length (Å) related to the H under study, the distances between the atoms and CPs (|X-CP|, X = O or H, Å), electron density ρ (a.u.), Laplacian density at the CP position $\nabla^2\rho$ (in a.u.), and bond ellipticity (ELLI) are given. The shortest HB for each H type is given in italics. H_b, O_w, and O_z are for bridged proton, H_2O, and zeolite oxygen, respectively.

HBs as in NaNAT and BaEDI. Depending on the dimension of the zeolite system, we applied more or less complete PHF optimizations of the zeolite structures including adsorbed H_2O molecules with the exception of LiBIK, for which we accepted the XRD model from the literature. With the PHF approach at the split valence plus polarization basis set level, we then computed electronic properties as the quadrupole coupling constants and EFG anisotropy to analyze the similarity between the properties of H_2O adsorbed in different zeolites and H_2O in liquid and solid states. The variation of the calculated atomic properties were illustrated using the quadrupole coupling constants $C_{qq}(^2H, ^{17}O)$ and the EF values. We observed a common (before and after optimization) behavior of $C_{qq}(^2H)$ with respect to the water O—H bond length of the adsorbed H_2O molecules for all H types irrespective of the different O—H coordination to the framework oxygens. Analogous quadratic type $C_{qq}(^2H)$ decrease with O—H was mentioned by Alfredsson and Hermansson [16] for isolated H_2O. We observed appreciable differences between the C_{qq} values of the ^2H atoms nonparticipating or participating in the 1-D water chains. The "chain" protons have properties that approach the ones of the ^2H atoms in ice or liquid water confinement. Their property variations are, however, smaller than those required for H_2O to achieve an "ice-like" state. One can conclude that hydrogen bonding to the zeolite oxygens or to an O

atom of a neighbor H_2O molecule leads to similar variations of the H_2O properties.

Two types of correlations between the EF absolute values at the H_2O proton position |EF(H)| and the water |OH| bond length and between the absolute values of the EF at the H_2O oxygen position |EF(O)| and the water HOH valence angle were observed for both the PHF-optimized and XRD models. Both correlations confirm the local character of the EF, which is determined by the closest atoms to the adsorbed H_2O molecules, i.e., H atoms for O and O atom for H, while the EF contribution from the zeolite framework is minor. This observation suggests that the EF does not play a dominant role in the preferential localization of adsorbed H_2O. The consideration of a representative series of cationic forms with more diverse adsorbed H_2O geometries should validate this idea.

We also showed that the H_2O adsorbed optimized geometries were less distorted as compared to the ones observed by X-ray; the water H—O—H valence angle is larger than in the gas state. The longer O—H bond lengths as compared to the gas state could not clearly be estimated with the STO-3G basis set used for the PHF optimization. In the LiABW case only, where the XRD water geometry is strongly perturbed as compared to the gas state, the PHF-optimized model is more stable than the initial XRD model. The O—H distance is overestimated with the STO-3G basis as compared to the one obtained by single-point PHF calculations with the 6-21G*(O, H) basis set. That is why the PHF total energies optimized with the STO-3G basis for the NaNAT and BaEDI zeolites are higher than those of the initial XRD models. The scaling of the PHF optimized water geometry (of the OH bond lengths only) for the BaEDI zeolite on the basis of gas-state STO-3G/6-21G* calculations allowed us to obtain a more stable model than the XRD model. Similar types of scaling procedures will be applied for all other zeolites studied in the future.

ACKNOWLEDGMENTS

The authors thank the FUNDP for the use of the Namur Scientific Computing Facility (SCF) Centre. They are grateful for the partial support of the Interuniversity Research Program on "Quantum Size Effects in Nanostructural Materials" (PAI/IUAP 5/01). The authors thank Professor C. Gatti for useful advice and Professor C. Lecomte and Dr. F. Porcher of the Université Henry Poincaré, Nancy, for fruitful discussions.

References

1. Cohen de Lara, E.; Delaval, Y. J Chem Soc Faraday Trans II 1978, 74, 790.
2. Marra, G. L.; Fitch, A. N.; Zecchina, A.; Ricchiardi, G.; Salvalaggio, M.; Bordiga, S.; Lamberti, C. J Phys Chem B 1997, 101, 10653.
3. Smith, L.; Cheetham, A. K.; Morris, R. E.; Marchese, L.; Thomas, J. M.; Wright, P. A.; Chen, J. Science 1996, 271, 799.
4. Jeanvoine, Y.; Ángyán, J. G.; Kresse, G.; Hafner, J. J Phys Chem B 1998, 102, 7307.
5. Termath, V.; Haase, F.; Sauer, J.; Hutter, J.; Parinello, M. J Am Chem Soc 1998, 120, 8512.
6. Ghermani, N. E.; Lecomte, C.; Dusausoy, Y. Phys Rev 1996, B53, 5231.
7. Krogh Andersen, E.; Ploug-Sorensen, G. Z Kristallogr 1986, 176, 67.
8. Kvick, Å; Smith, J. V. J Chem Phys 1983, 79, 2356.
9. Ståhl, K.; Kvick, Å; Ghose, S. Zeolites 1989, 9, 303.
10. Espinosa, E.; Souhassou, M.; Lachekar, H.; Lecomte, C. Acta Crystallogr 1999, B55, 563.
11. Bouhmaida, N.; Ghermani, N. E.; Lecomte, C.; Thalal, A. Acta Crystallogr 1999, A55, 729.
12. Fois, E.; Tabacchi, G.; Quartieri, S.; Vezzalini, G. J Chem Phys 1999, 111, 355.
13. Fois, E.; Gamba, A.; Tabacchi, G.; Quartieri, S.; Vezzalini, G. Phys Chem Chem Phys 2001, 3, 4158.
14. Fois, E.; Gamba, A.; Tabacchi, G.; Quartieri, S.; Vezzalini, G. J Phys Chem B 2001, 105, 3012.
15. Dovesi, R.; Saunders, V. R.; Roetti, C.; Causà, M.; Harrison, N. M.; Orlando, R.; Aprà, E. CRYSTAL95 1.0 User's Manual; University of Torino: Torino, Italy, 1996.
16. Alfredsson, M.; Hermansson, K. Chem Phys 1999, 242, 161.
17. Camus, S.; Harris, K. D. M.; Johnston, R. L. Chem Phys Lett 1997, 276, 186.
18. Larin, A. V.; Vercauteren, D. P. Int J Quantum Chem 2001, 82, 182.
19. Bader, R. F. W. Atoms in Molecules: A Quantum Theory; The International Series of Monographs in Chemistry; Clarendon Press: Oxford, UK, 1995.
20. Gatti, C. TOPOND-96. User's Manual; CNR-CSRSRC: Milan, Italy, 1996.
21. Frisch, M. J.; Trucks, G. W.; Schlegel, H. B.; Scuseria, G. E.; Robb, M. A.; Cheeseman, J. R.; Zakrzewski, V. G.; Montgomery, J. A. Jr.; Stratmann, R. E.; Burant, J. C.; Dapprich, S.; Millam, J. M.; Daniels, A. D.; Kudin, K. N.; Strain, M. C.; Farkas, O.; Tomasi, J.; Barone, V.; Cossi, M.; Cammi, R.; Mennucci, B.; Pomelli, C.; Adamo, C.; Clifford, S.; Ochterski, J.; Petersson, G. A.; Ayala, P. Y.; Cui, Q.; Morokuma, K.; Malick, D. K.; Rabuck, A. D.; Raghavachari, K.; Foresman, J. B.; Cioslowski, J.; Ortiz, J. V.; Baboul, A. G.; Stefanov, B. B.; Liu, G.; Liashenko, A.; Piskorz, P.; Komaromi, I.; Gomperts, R.; Martin, R. L.; Fox, D. J.; Keith, T.; Al-Laham, M. A.; Peng, C. Y.; Nanayakkara, A.; Challacombe, M.; Gill, P. M. W.;

Johnson, B.; Chen, W.; Wong, M. W.; Andres, J. L.; Gonzalez, C.; Head-Gordon, M.; Replogle, E. S.; Pople, J. A. Gaussian 98, Revision A.7; Gaussian, Inc.: Pittsburgh, PA, 1998.

22. Larin, A. V.; Vercauteren, D. P. Stud Surf Sci Cat 2002, 142B, 1987.
23. Karadakov, P. B. J Mol Struct 2002, 602/603, 293.
24. Quartieri, S.; Sani, A.; Vezzalini, G.; Galli, E.; Fois, E.; Gamba, A.; Tabacchi, G. Micro Meso Mater 1999, 30, 77.
25. Press, W. H.; Flannery, B. P.; Teukolsky, S. A.; Wetterling, W. T. Numerical Recipes; Cambridge University Press: New York, 1988.
26. Ugliengo, P.; Viterbo, D.; Chiari, G. Z Kristallogr 1993, 207, 9.
27. Larin, A. V.; Vercauteren, D. P. Stud Surf Sci Cat 2001, 135, 263.
28. Cerius 2, User's Guide, Version 4.0.0; MSI: San Diego, 1997.
29. Peschke, M.; Blades, A. T.; Kebarle, P. J Phys Chem A 1998, 102, 9978.
30. Rodriguez-Cruz, S. E.; Jockusch, R. A.; Williams, E. R. J Am Chem Soc 1999, 121, 1986.
31. Otero Areán, C.; Manoilova, O. V.; Rodriguez-Delgado, M.; Tsyganenko, A. A.; Garrone, E. Phys Chem Chem Phys 2001, 3, 4187.
32. Yamazaki, T.; Watanuki, I.; Ozawa, S.; Ogino, Y. Bull Chem Soc Jpn 1988, 61, 1039.
33. Larin, A. V.; Vercauteren, D. P. Int J Quantum Chem 2001, 83, 70.
34. Larin, A. V.; Vercauteren, D. P. J Mol Cat A 2001, 168, 123.
35. Porcher, F.; Larin, A. V.; Aubert, E.; Vercauteren, D. P.; Souhassou, M.; Lecomte, C.; Philippot, E. Euroresco Conference "Zeolite Molecular Sieves—Euroconference on Isomorphous Substitution by Transition Metals"; Obernai, France, 2002.